

DOI: 10.1002/adma.200601908

Piezoelectric Gated Diode of a Single ZnO Nanowire**

By Jr H. He, Cheng L. Hsin, Jin Liu, Lih J. Chen,* and Zhong L. Wang*

One-dimensional (1D) semiconducting nanostructures,^[1] such as nanowires (NWs) and nanobelts (NBs), are fundamental building blocks for constructing nanoscale electronic devices^[2] because of their small size and the enhanced charge carrier mobility owing to 1D confinement. Considerable efforts have been devoted to energy-band engineering by doping for controlling their electrical properties and assembling NWs into increasingly complex structures.^[2a,2b,2d,3] The rectifier, a fundamental device for electronics, normally consists of a *p-n* junction diode. The role of the dopants is the formation of a *p-n* junction and creation of an electrostatic potential energy barrier at the junction.

ZnO exhibits the most diverse and abundant configurations of nanostructures known so far, such as NWs, NBs, nanosprings, nanorings, nanobows, and nanohelices.^[4] Numerous studies based on ZnO nanostructures have demonstrated novel applications due to their semiconducting and piezoelectric properties.^[1a,1e,5] For ZnO, *n*-type conductivity is relatively easy to realize via excess Zn, or with Al, Ga, or In doping, but *p*-type doping has only recently been achieved.^[6] This leads to the conclusion that the generation of *p*-type material is one of the last major obstacles hindering the development of ZnO-based electronic and optoelectronic devices. There are many possible strategies for doping ZnO in order to make *p-n* junctions for advancing the technological uses of ZnO-based electronic and optoelectronic devices.^[6]

As an alternative approach for achieving *p*-type ZnO, we have been exploring the potential of coupling the piezoelectric effect with the semiconducting property of ZnO to achieve a few unique applications. In this Communication, we show how an *n*-type ZnO NW can be used to produce a *p-n* junction that serves as a diode. Our design is based on the mechanical bending of a ZnO NW. As a result, the potential energy barrier induced by piezoelectricity (ψ_{PZ}) across the bent NW governs the electrical transport through the NW. To quantify ψ_{PZ} , the current–voltage (*I*–*V*) characteristics re-

ceived at different levels of deformation were included in theoretical calculations. The magnitude of the piezoelectric barrier dominates the rectifying effect. The rectifying ratio could be as high as 8.7:1 by simply bending a NW. The operation current ratio of a straight to a bent ZnO NW could be as high as 9.3:1 at reverse bias. This also shows that the NW can serve as a random access memory (RAM) unit.

Figure 1a shows a typical scanning electron microscopy (SEM) image of a well-aligned ZnO NW array. Figure 1b shows a typical transmission electron microscopy (TEM) image of a single ZnO NW. The corresponding selected-area electron diffraction pattern (Fig. 1c) confirms that the phase of the NWs is hexagonal wurtzite-structured ZnO. Figure 1d is a high-resolution TEM (HRTEM) image from the outlined region indicated in Figure 1b. Figure 1c and d shows that the ZnO NWs are single-crystalline and free of dislocations. The growth direction of the ZnO NW was determined to be [0001].

In situ *I*–*V* measurements and the manipulation of ZnO NWs were carried out in a multiprobe nanoelectronics measurement (MPNEM) system. The two-terminal method was applied for electrical transport measurements at high vacuum to minimize influences from the environment. The tungsten nanotip used for measuring the electrical transport of a nanowire was precoated with a Ti/Au (30 nm:30 nm) film by electron-beam evaporation to obtain Ohmic contact between Ti and ZnO. Creating Ohmic contact is a key step for the measurements. Focusing the NW and the W nanotip in the

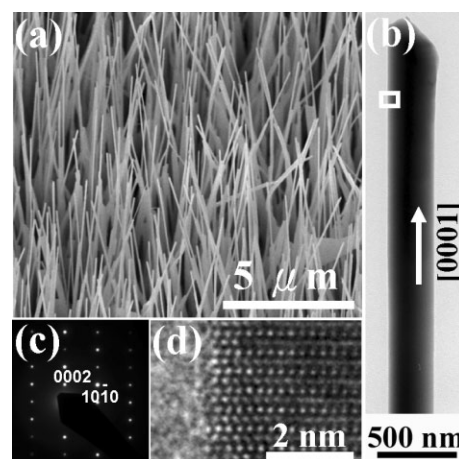


Figure 1. a) An SEM image of a well-aligned ZnO NW array; b) TEM image of a single ZnO nanorod; c) Corresponding selected-area electron diffraction pattern, and d) high-resolution TEM image of the ZnO nanowire at the boxed region marked in (b).

[*] Prof. Z. L. Wang, Dr. J. H. He, J. Liu
School of Materials Science and Engineering
Georgia Institute of Technology
Atlanta, GA 30332-0245 (USA)
E-mail: zhong.wang@mse.gatech.edu

Prof. L. J. Chen, Dr. J. H. He, C. L. Hsin
Department of Materials Science and Engineering
National Tsing Hua University
Hsinchu 300 (Taiwan)
E-mail: ljchen@mx.nthu.edu.tw

[**] This research was supported by the NSF, DARPA, NASA, NIH, and NSC.

MPNEM system simultaneously in the same focal plane guaranteed that they were contacted and placed at the same height on the surface of the Si_3N_4 layer.

Figure 2 schematically illustrates a manipulator making a two-terminal connection to a single ZnO NW to measure its electrical transport properties. The lower nanotip is used to apply the voltage and measure the current through the NW. By controlling the lateral and longitudinal motions of the two nanotips with highly sensitive and sophisticated probing tech-

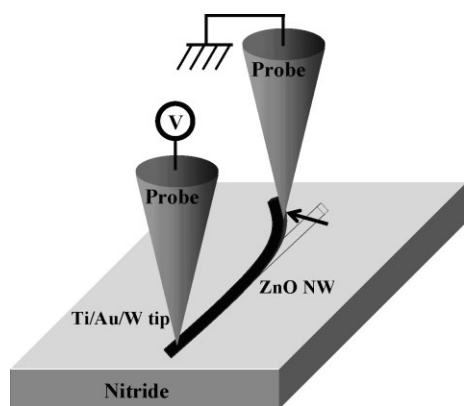


Figure 2. Schematic diagram of the nanomanipulation and in situ I - V measurement setup in the MPNEM system, in which SEM, which can provide higher resolution, is employed to locate the nanowires and navigate the nanotip to a certain region.

niques, the manipulation of the NW and its I - V measurements were carried out in situ in the scanning electron microscope. To eliminate the effect from the electron beam in the SEM instrument, the electron beam was turned off when taking I - V measurements. The I - V characteristics were measured by sweeping the voltage from -5 to $+5$ V. After the measurement, the electron beam was turned on again to ensure the preservation of the shape and position of the NW.

The NW was then bent further by moving the upper nanotip under the direct-imaging condition. Following the I - V measurements, the sequential images of the bent NW were captured. The typical sequence of the ZnO NW at various bending angles is shown in the left column of Figure 3. Their corresponding I - V characteristics are presented on the right-hand side of Figure 3. At the first contact of the NW with the W tip (Fig. 3a), the NW was already bent a little because a pushing force was necessary for good electrical contact. The corresponding linear and symmetric I - V characteristic shows that the Ti/Au-to-ZnO NW is an Ohmic contact rather than a double (back-to-back) Schottky contact (Fig. 3b). As the bending proceeded (Fig. 3c, e, and g), the electric current dropped significantly with negative bias (Fig. 3d, f, and h, respectively), exhibiting asymmetric I - V behaviors with the increased strain. It can be seen clearly that the nanotips were firmly attached to the NW without sliding, indicating that the contacts were well retained during the bending process and should not cause any change in contact resistance or contact

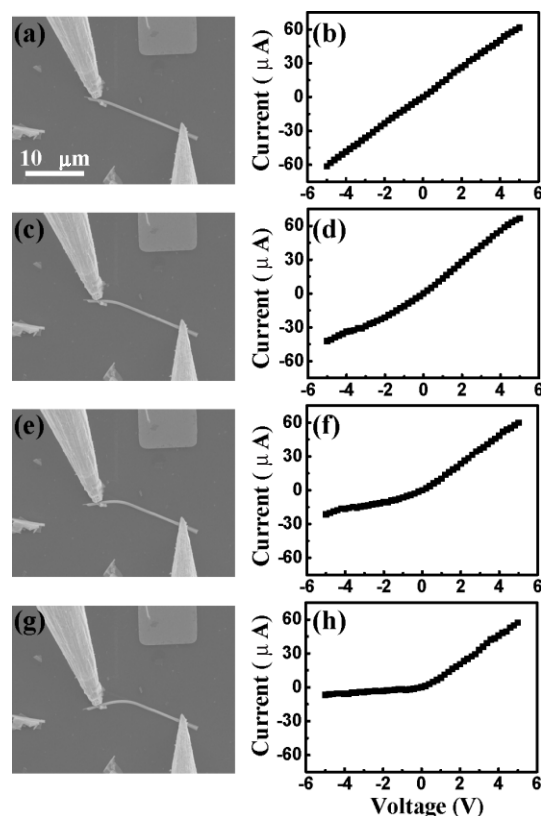


Figure 3. The sequence of SEM images of the ZnO NW at various bending angles is shown on the left (a, c, e, g). The corresponding I - V characteristics are shown on the right (b, d, f, h).

area under bending. The reverse current dropped severely at reverse bias voltage when the NW was bent further. When the NW was under significant bending, the reverse current at -5 V bias could be as low as ca. $6.6 \mu\text{A}$, and the rectifying ratio at ± 5 V was up to 8.7:1. Due to the large elasticity of the NW, the measurements of these devices are reversible. The details of electric current at reverse bias and the rectifying ratio at ± 5 V under a continuously changing bending curvature are listed in Table 1. The potential energy barrier height induced by piezoelectricity will be discussed in detail later. The ZnO NW under bending shows certain rectifying I - V characteristics, similar to the result for a p - n junction. The substantial bending of the NW and the absence of a symmetric I - V

Table 1. The electric current at reverse bias and the rectifying ratio at ± 5 V under a continuously changing bending curvature, together with an estimation of the piezoelectric potential energy barrier, ψ_{PZ} . The measurement stages #1, #2, #3, and #4 correspond to Fig. 3a, c, e, and g, respectively.

Measurement stage	I at -5 V [μA]	Rectifying ratio	Piezoelectric potential energy barrier [meV]
#1	-61.4	1:1	-
#2	-42.0	1.6:1	9.5
#3	-21.3	2.8:1	27.37
#4	-6.6	8.7:1	57.66

characteristic suggest that electrical transport in the NW may be governed by an internal field created by bending.

We have recently shown that a bent ZnO NW can produce a piezoelectric electric field (E_{PZ}) along and across the NW due to the strain-induced piezoelectric effect.^[5b] The discussion of the observed phenomena is meant as an illustration of the physical process and principle rather than as a rigorous numerical calculation. We simply consider the piezoelectric effect introduced in a single NW as a result of elastic deformation. For a simulated case in a NW of ca. 490 nm thickness and 21 μm length under the displacement of an external force F from the nanotip applied at the surface of the NW (Fig. 3g), the deflection of the ZnO NW creates a strain field. The outer surface is stretched (positive strain ε) and the inner surface is compressed (negative ε) in the area in contact with the nanotip, as shown in Figure 4a. The magnitude of the deflection increases with the degree of bending, resulting in an increase in strain field. An electric field E_{PZ} along the NW is then created inside the NW through the piezoelectric effect, $E_{PZ} = \varepsilon/d$, where d is the piezoelectric coefficient. The piezoelectric field direction is closely parallel to the NW direction (z -axis) at the outer surface and antiparallel to the z -axis at the inner surface. With the increase in bending of the NW, the density of

the piezoelectric charges on the surface also increases. The potential is created by the relative displacement of the Zn^{2+} cations with respect to the O^{2-} anions, a result of the piezoelectric effect in the wurtzite crystal structure; thus, these ionic charges cannot freely move and cannot recombine without releasing the strain. The potential difference is maintained as long as the deformation is in place.

We assume that, before bending, there is no energy barrier except for the contact resistance between Ti and ZnO. When the nanotip pushes a NW and bends it, as shown in the schematic plot in Figure 2, a positive potential is produced at the stretched side of the NW due to the piezoelectric effect. As a result, an energy barrier is produced at the interface between the tip and the NW, with the NW being at the higher potential, as illustrated in Figure 4b. Note that the actual potential distribution is not fixed due to the nonuniform distribution of strain. However, for ease of comprehension, we simplify the potential distribution here. The schematic diagrams depicting the principle of operation are shown in Figure 4c and d. For the bent ZnO NW under forward bias, the electrons have not been blocked by this energy barrier. On the other hand, under reverse bias, electrons need to overcome the energy barrier resulting from the piezoelectric electric field. This energy diagram corresponds well to the result of electric transport measurements on bent ZnO. Such an energy barrier effectively serves as a p - n junction barrier at the interface, resisting the current flow from the tip to the NW but allowing current to flow from the NW to the tip. The magnitude of the barrier increases with the increase in the degree of bending, resulting in a drastic increase of rectifying effect due to the piezoelectric potential energy barrier. This is a simple piezoelectric gated diode. To quantify the barrier height produced by piezoelectricity, we assume here that the electric current also follows the typical I - V characteristics of a diode. The reverse current is given by Equation 1:

$$I_s = A e^{-\psi_{PZ}/kT} (e^{eV/kT} - 1) \quad (1)$$

where ψ_{PZ} is the potential energy barrier resulting from piezoelectricity, I_s is the reverse saturation current, V is the applied voltage, e is the electronic charge, k is the Boltzmann constant ($8.617 \times 10^{-5} \text{ eV K}^{-1}$), T is the absolute temperature, and A is a constant. We consider the electric current at -5 V and room temperature with bending degree, thus the above equation can be simplified as follows since the $(e^{eV/kT} - 1)$ term is a constant:

$$I_s = A^* e^{-\psi_{PZ}/kT} \quad (2)$$

where A^* is a constant. We assume that the current is $61.4 \mu\text{A}$ as ψ_{PZ} is zero when there is no deflection observed (Table 1); thus A^* is determined to be $61.4 \mu\text{A}$. Therefore, by the given electric current from Table 1, this could lead to an estimation of ψ_{PZ} to be ca. 9.82 meV for stage #2, 27.37 meV for stage #3, and 57.66 meV for stage #4, respectively. These are

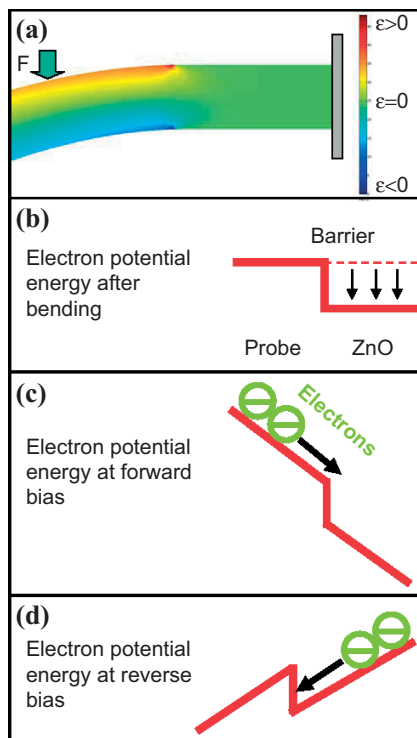


Figure 4. a) Longitudinal strain (ε) distribution along a ZnO NW as a result of the piezoelectric effect when bent by a nanotip, with the stretched and compressed side surfaces being under positive and negative strain, respectively. Schematic energy diagram of ZnO NW accounting for the applied bias and the piezoelectric field. b) Energy barrier built at the nanotip/nanowire interface due to the piezoelectric potential (V^*) at the stretched side. c) Current flow under forward bias. d) Current flow under reverse bias.

listed in Table 1. Theoretical calculations together with experimental measurements confirm that the magnitude of the piezoelectric barrier dominates the rectifying effect. The barrier height we have estimated here agrees well with the electrical energy output from a single ZnO NW for use as a NW-based piezoelectric power nanogenerator.^[5b]

Moreover, a mechanical force was applied to control the electric output to determine the “1” and “0” states (ON and OFF states, respectively; Fig. 5). Each NW array corresponds to a device element for memory application. With an applied -5 V bias, by applying a mechanical force, the operating current ratio between a straight and bent ZnO NW could be as high as 9.3:1. This leads to the appearance of well-defined “1” and “0” states; that is, the shape will be highly sensitive to the electric current due to piezoelectricity. A device element could be switched between these “1” and “0” states by mechanical force to receive different electric signals. On the basis of this switching mode, we can characterize the elements as nanoscale electromechanical devices.

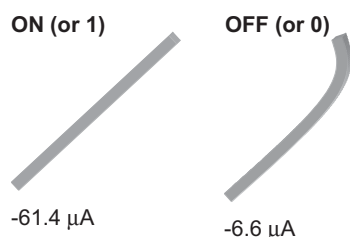


Figure 5. Structures of the ZnO NW device element for RAM application in the “ON” (left) and “OFF” (right) states, showing the current under -5 V bias in each of the states, which gives an ON/OFF ratio of 9.3:1.

In summary, we have performed nanomanipulation to measure the in situ I - V characteristics of a single ZnO NW. The electric transport was dominated by the strain-induced piezoelectric characteristic of ZnO. It has been demonstrated that a single ZnO NW can be a rectifier simply by mechanically bending it, similar to a p - n junction based diode. To quantify the barrier height produced by piezoelectricity, the I - V characteristics received at different levels of deformation were tied in with theoretical calculations. In addition, under appropriate bending and voltage control, each NW array could correspond to a device element for RAM application.

Experimental

The ZnO NWs used for the experiments were grown using a vapor-liquid-solid process. A 2 nm thick Au thin film, which serves as the catalyst for growth, was deposited onto a (1120)Al₂O₃ substrate

at room temperature in an electron-beam evaporation system (ca. 5×10^{-6} Torr; 1 Torr = 133 Pa). The experimental apparatus includes a horizontal tube furnace, a rotary pump system, and a gas-supply system. A mixture of commercial ZnO and graphite powders in a ratio of ZnO/C = 4:1 was placed in an alumina boat, which was heated to a peak temperature of 1100 °C. The Al₂O₃ substrate was placed in the temperature zone of ca. 800 °C for collecting the ZnO nanostructures. After the tube had been evacuated to a pressure of 1×10^{-3} Torr, the samples were heated to 1100 °C at a rate of 5 °C min⁻¹ and held at 1100 °C for 60 min with a carrier gas of Ar and O₂ flowing through the tube. The substrate-bound ZnO NW arrays were mechanically scraped off and sonicated in ethanol, then deposited on a Si substrate covered with a Si₃N₄ layer as insulator.

The scraped NWs were placed on carbon-coated copper grids for TEM characterization. Morphological studies of grown ZnO nanostructures were performed with a JEOL 2010 TEM instrument operating at 200 kV and a JEOL JSM-6500 field-emission scanning electron microscope. HRTEM images were obtained by using a JEOL JEM-3000F field-emission TEM instrument, with a point-to-point resolution of 0.17 nm, operating at 300 kV.

The performance of in situ I - V measurements and the manipulation of ZnO NWs were carried out in an MPNEM system. The two-terminal method was applied for electrical transport measurements. As all of the procedures were carried out at a pressure of ca. 5×10^{-4} Pa, possible influences from the environment could be minimized. The MPNEM system is composed of several subsystems: 1) field-emission SEM gun (JEOL JSM-7000F); 2) nanomanipulator system (four-needle experimental probing device, Kammrath & Wiess GmbH); and 3) an I - V measurement system (Keithley Model 4200-SCS).

Received: August 22, 2006

Revised: October 5, 2006

Published online: February 12, 2007

- [1] a) Z. L. Wang, *J. Mater. Chem.* **2005**, *15*, 1021. b) J. T. Hu, T. W. Odom, C. M. Lieber, *Acc. Chem. Res.* **1999**, *32*, 435. c) P. D. Yang, *MRS Bull.* **2005**, *30*, 85. d) L. Samuelson, *Mater. Today* **2003**, *6*, 22. e) Z. L. Wang, *Mater. Today* **2004**, *7*, 26.
- [2] a) C. Yang, Z. Zhong, C. M. Lieber, *Science* **2005**, *310*, 1304. b) Y. Cui, C. M. Lieber, *Science* **2001**, *291*, 851. c) Y. Huang, X. Duan, Y. Cui, C. M. Lieber, *Nano Lett.* **2002**, *2*, 101. d) J. H. He, C. S. Lao, L. J. Chen, D. Davidovic, Z. L. Wang, *J. Am. Chem. Soc.* **2005**, *127*, 16376.
- [3] C. W. Zhou, J. Kong, E. Yenilmez, H. J. Dai, *Science* **2000**, *290*, 1552.
- [4] a) M. H. Huang, Y. Y. Wu, H. Feick, N. Tran, E. Weber, P. D. Yang, *Adv. Mater.* **2001**, *13*, 113. b) Z. W. Pan, Z. R. Dai, Z. L. Wang, *Science* **2001**, *291*, 1947. c) X. Y. Kong, Z. L. Wang, *Nano Lett.* **2003**, *3*, 1625. d) X. Y. Kong, Y. Ding, R. Yang, Z. L. Wang, *Science* **2004**, *303*, 1348. e) W. L. Hughes, Z. L. Wang, *J. Am. Chem. Soc.* **2004**, *126*, 6703. f) P. X. Gao, Y. Ding, W. J. Mai, W. L. Hughes, C. S. Lao, Z. L. Wang, *Science* **2005**, *309*, 1700.
- [5] a) M. H. Huang, S. Mao, H. Feick, H. Q. Yan, Y. Y. Wu, H. Kind, E. Weber, R. Russo, P. D. Yang, *Science* **2001**, *292*, 1897. b) Z. L. Wang, J. H. Song, *Science* **2006**, *312*, 242. c) J. H. Song, J. Zhou, Z. L. Wang, *Nano Lett.* **2006**, *6*, 1656. d) B. A. Buchine, W. L. Hughes, F. L. Degertekin, Z. L. Wang, *Nano Lett.* **2006**, *6*, 1155.
- [6] a) D. P. Norton, Y. W. Heo, M. P. Ivill, K. Ip, S. J. Pearton, M. F. Chisholm, T. Steiner, *Mater. Today* **2004**, *7*, 34. b) S. J. Pearton, D. P. Norton, K. Ip, Y. W. Heo, T. Steiner, *J. Vac. Sci. Technol. B* **2004**, *22*, 932.